J Mol Model (2012) 18:3243–3253
DOI 10.1007/s00894-011-1323-x

ORIGINAL PAPER

First- and second-row transition metal oxa-aza macrocyclic complexes: a DFT study of an octahedral conformation

Francisco C. A. Lima · Rommel B. Viana · Thais T. da Silva · Solange M. S. V. Wardell · Armando P. Nascimento do Filho · José Walkimar M. Carneiro · Moacyr Comar Jr. · Albérico B. F. da Silva

Received: 3 August 2011 / Accepted: 25 November 2011 / Published online: 15 January 2012

Abstract A theoretical study of structures of the 1,7,1 l,17-tetraoxa-2,6,12,16-tetraaza-cycloeicosane ligand ([20]$AneN_4O_4$) coordinated to Fe^{2+}, Co^{2+}, Ni^{2+}, Ru^{2+}, Rh^{2+}, and Pd^{2+} transition metals ions was carried out with the DFT/B3LYP method. Complexes were fully optimized in C_s symmetry with the metal ions coordinated either to nitrogen (**1a**) or oxygen atoms (**1b**). For all the cases performed in this work, **1a** was always more stable than **1b**. Considering each row it is possible to see that the binding energy increases with the atomic number. The M^{2+} cation binding energies increase in the following order: $Fe^{2+}<Ru^{2+}<Co^{2+}<Ni^{2+}<Rh^{2+}<Pd^{2+}$. In addition, it was observed the preference of Pd^{2+} and Rh^{2+} complexes for a tetrahedral arrangement, while Fe^{2+}, Ru^{2+}, Co^{2+}, Ni^{2+} complexes had a preference for the octahedral arrangement. From the orbital representation results, it was seen that **1b** unsymmetrical orbitals may influence the susceptibility over metal ions orientation toward heteroatoms orbitals.

Keywords Binding energy · Charge decomposition analysis · Covalent interactions · Ionic interactions · Oxa-aza macrocycles · Transition metal cations

F. C. A. Lima
Centro de Ciências da Natureza, Departamento de Química,
Universidade Estadual do Piauí,
Teresina, PI, Brasil

R. B. Viana · A. B. F. da Silva (✉)
Departamento de Química e Física Molecular,
Instituto de Química de São Carlos, Universidade de São Paulo,
São Carlos, SP, Brasil
e-mail: alberico@iqsc.usp.br

T. T. da Silva · A. P. N. do Filho · J. W. M. Carneiro
Departamento de Química Inorgânica, Instituto de Química,
Universidade Federal Fluminense,
Niterói, RJ, Brasil

S. M. S. V. Wardell
FioCruz - Fundação Oswaldo Cruz,
Instituto de Tecnologia em Fármacos,
FarManguinhos,
Rio de Janeiro, RJ, Brasil

M. Comar Jr.
Universidade Federal de São João Del Rei,
Divinópolis, MG, Brasil

Introduction

Macrocycles with heteroatoms such as nitrogen and oxygen have found wide applications in extensive branches of science. Azamacrocycles and oxa−aza macrocycles have been applied as chelating agents for metals [1, 2], organic cations [1, 2] and radioisotopes [3, 4]. Anti-HIV activity has also been observed in azamacrocycles and their metal complexes [5–7], while oxa−aza macrocycles has also been employed in the development of a new selectivity electrode to the determination of nitrate in vegetable and bottled mineral water [8].

Special interest has been concerned over heteromacrocycle systems due to their ability to recognize metal ions. Heteromacrocycles metal ion selectivity characteristics is assigned to the (a) ligand−specific affinity [9], (b) the nature and arrangement of donor atoms [10, 11], (c) the cavity size [9, 11], (d) and the cavity charge distribution, i.e., the donor capacity of heteroatoms [9, 11]. Due to this reason, heteroatom macrocyclic selectivity has been assessed by experimental and theoretical procedures to different transition metal ions [12–15]. Another important aspect over the macrocyclic chelating

efficiency is its conformation. For some macrocycles, the general arrangement remains the same before and after transition metal ion complexation [9]. Depending on the conformation before the complexation, the system can be recognized as more or less efficient ligand [11].

In a recent work, the synthesis [16] and coordination chemistry [17] of the 1,7,1 l,17-tetraoxa-2,6,12,16-tetraazacycloeicosane macrocyclic systems ([20]AneN_4O_4 and [20]AneO_4N_4) were reported. Although the coordination chemistry of macrocycles containing both nitrogen and oxygen atoms is well known [18], the mixed macrocycle [20]AneN_4O_4 (and [20]AneO_4N_4) is the first one with potential nitrogen and oxygen atom donors. Depending on the surrounding environment and the metal cation, there is the possibility of switching between nitrogen and oxygen donor (see Scheme 1). Kuksa *et al.* [17] demonstrated that when [20]AneN_4O_4 complexes with Ni (II) ion a hexa-coordination to four nitrogen atoms with two crystallization water in pseudo axial positions showing an octahedral arrangement is observed. It is important to mention that only a structural investigation of this complex was performed and there is an absence of some molecular characteristics of this kind of system.

The purpose of the present work is to perform a theoretical investigation of [20]AneN_4O_4 and [20]AneO_4N_4 complexes with first- and second-row transition metals. The nature of the interactions between these kind of systems and metal ions of the first (Fe, Co, Ni) and second (Ru, Rh, Pd) transition series is unknown. In this investigation, we quantified the relative complexation energy of the selected cations and identified whether the complexation occurs preferentially via the nitrogen or oxygen atoms. It is important to say that this work will focus on the octahedral arrangement and due to this reason it will be considered two water molecules in the axial positions as was previous observed by Kuksa *et al.* [17]. A detailed understanding of what happens to a molecule after the complexation, and the knowledge at the microscopic level which controls their capability to form complexes with the transition metals, increases our ability to design efficient novel molecular recognition systems. Therefore, this work will present a clear indication of the potential of the macrocycle [20]AneN_4O_4 as a metal sensor.

Theoretical methodology

Density functional theory (DFT) calculations were performed in this work using the Gaussian 03 program [19]. Optimized molecular geometries were calculated in vacuum by using the hybrid B3LYP [20, 21] exchange-correlation functional with the LANL2DZ pseudopotential. B3LYP includes the functional developed by Becke [22], Lee-Yang-Parr [23] and Vosko-Wilk-Nusair [24] correlation functionals. All the fully optimized geometries were characterized by vibrational frequency calculations, which showed only real frequencies. Zero-point vibrational energies were estimated based on the B3LYP frequency

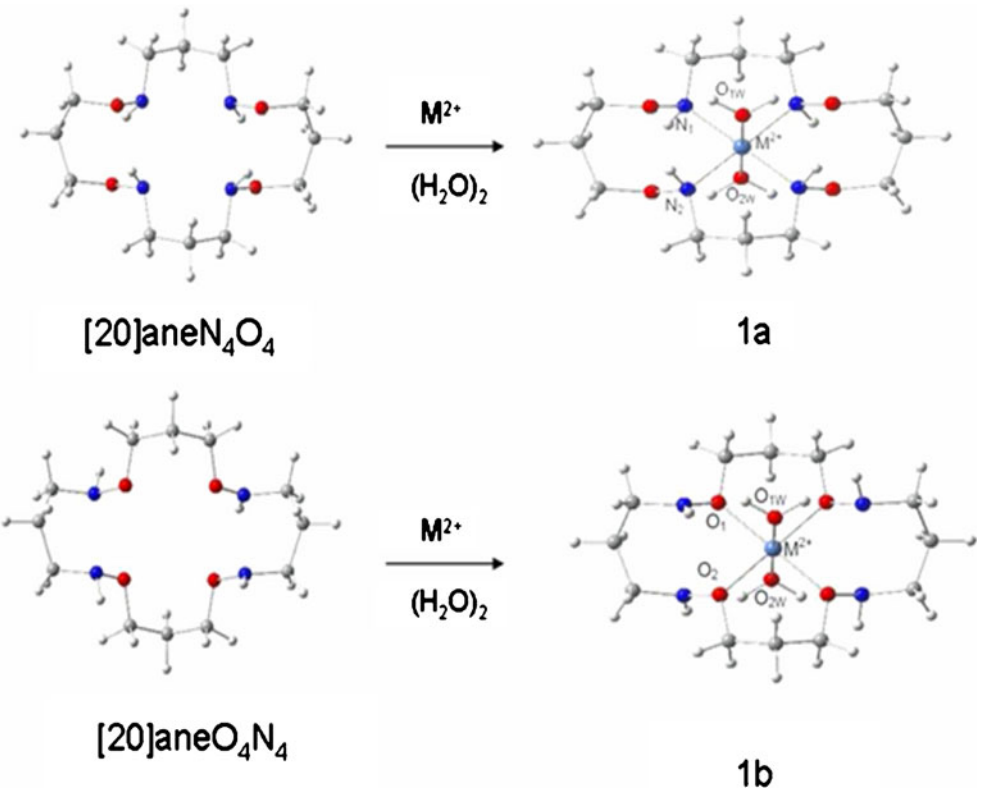

Scheme 1 Metal and two water molecules coordination for [20]aneN$_4$O$_4$ and [20]aneO$_4$N$_4$

calculation (unscaled) using the same basis set as for the geometry optimization calculations. GDIIS algorithim [25, 26] was also employed in each calculation.

Two types of complexes were evaluated in the present work. It was considered where nitrogens are the donor atoms ([20]AneN$_4$O$_4$, **la**) and where oxygens are the donor ones ([20]AneO$_4$N$_4$, **lb**). **la** starting geometry was designed with C$_s$ symmetry based on the experimental X-ray diffraction structure determination of the octahedral Ni^{2+} complex of [20]AneN$_4$O$_4$. The macrocyclic dihedral angles were settled up according to the experimental angles. The main conformational features of the calculated complexes reproduced the experimental data. The starting geometries with others metal than nickel were obtained by the replacement of the corresponding Ni^{2+} cation by M^{2+} ones followed by full geometry optimization. Due to the absence of experimental data for the macrocyclic complexes with oxygen as donor atoms, we took [20]AneN$_4$O$_4$ as the starting point and changed the nitrogen by oxygen and performed the optimization.

The main aims of our work are to evaluate the macrocyclic metal ion selectivity as well as to understand the nature of the metal-ligand (N, O) chemical bond in the complexes in terms of donation from the ligand to metal and back-donation from the metal to the ligand, as calculated with the AOMix-CDA program.[20]

The macrocyclic coordination ability with different metal cations is given in a first approximation by the interaction energy, as defined in Eq. 1.

$$E_{INT} = E_{COMPLEX} - (E_{LIGAND} + E_{METAL} + 2E_{H2O}) \quad (1)$$

$E_{COMPLEX}$ is the energy of **la** or **1b** complex with different metal cations. While E_{LIGAND} is the energy of the macrocyclic ligand, E_{H2O} is the energy of the water molecule, and E_{METAL} is the metal cation energy. It is important to mention that counterpoise correction was not taken into account in the E_{INT} result.

Molecular orbital (MO) compositions and the overlap populations were calculated using the *AOMix* program [27, 28]. Atomic charges were calculated using natural population analyses (NBO) [29], as implemented in the *Gaussian 03* software. The analysis of the MOs compositions in terms of occupied and unoccupied fragment molecular orbitals (OFOs and UFOs, respectively) and the charge decomposition analysis (CDA) were performed using *AOMix-CDA* [30]. CDA is a valuable tool in analyzing the chemical bonding between the metal and the ligand in terms of metal→ligand donation and metal←ligand back-donation. This analysis was performed to quantify the charge donation and back-donation between the metal, macrocycle and the two water molecule fragments of the complexes studied in this work. It is important to mention that the CDA procedure between ligand-to-metal donation and metal-to-ligand back-donation is not the same as the net charge transfer between the metal and the ligand fragments. In fact, the CDA analysis only gives reasonable estimates of the donation and back-donation interactions if the electronic polarization is absent or if it is sufficiently small [27] since this is associated with the fact that in CDA [31] the terms donation and back-donation correspond to an overall reorganization of the electronic density, which includes the interfragment reorganization as well as charge transfer (CT) [27]. The Mayer bond orders [32–35] were calculated as implemented in AOMix-L [29].

Results and discussions

An analysis of the atomic charges before complexation was performed and it is shown in Table 1. From Table 1 we can see that the macrocycles show different negative charge values on the heteroatoms. In [20]AneN$_4$O$_4$ macrocycle, the oxygen atoms are more negatively charged than the nitrogen ones; and in [20]AneO$_4$N$_4$, the nitrogen atoms have a high negative charge due to the charge transfer from oxygen atoms to nitrogen ones. While [20]AneN$_4$O$_4$ geometry presented a nearly C$_s$ symmetry, [20]AneO$_4$N$_4$ shows an altered one, leading to a more deformed arrangement (see Scheme 1). In addition, [20]AneO$_4$N$_4$ is 7.2 kcal.mol^{-1} more stable than [20]AneN$_4$O$_4$. Figure 1 shows the conformational arrangements adopted by the free macrocycles and the cross distances between the heteroatoms.

A comparison between theoretical and X-ray data [17] for the Ni^{2+} complex was also performed in this work. Table 2 shows that the calculated N1-Ni bond lengths are close to those observed experimentally and the N1-Ni-N2 bond angles of the metal-coordination environment are also close to the experimental values with a difference of only 7°. While N1-Ni-O$_{2W}$ and N2-Ni-O$_{1W}$ experimental values are 89.7 and 88.6°, the calculated ones are 88.2 and 88.1,° respectively. In addition, the calculated angles between the two water molecules and the nickel ion is only 0.036° lower. Therefore, it can also be seen from Table 1 that our DFT

Table 1 NBO atomic charges and absolute energies of the macrocycles

Macrocycle	Charge	Energy (Hartree)
[20]AneN$_4$O$_4$		
Nitrogen[a]	−1.611	−993.19359
Oxygen[b]	−1.888	
[20]AneO$_4$N$_4$		
Nitrogen[a]	−1.975	−993.21484
Oxygen[b]	−1.609	

[a,b] Sum over the four nitrogen atoms and the four oxygen atoms, respectively

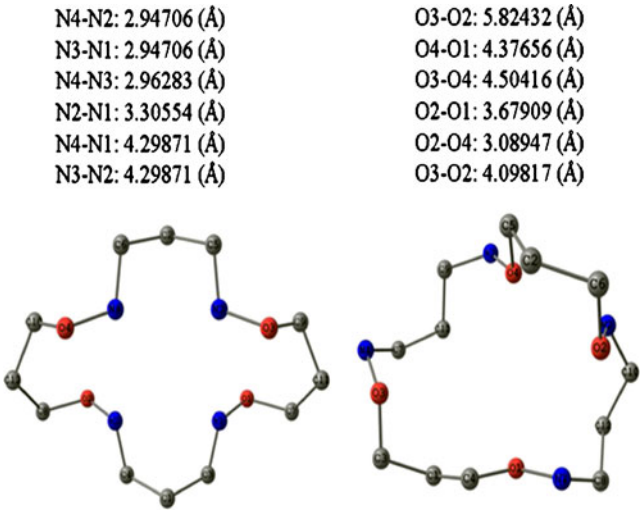

Fig. 1 Conformational arrangements and the bond length between heteroatoms of the [20]AneN4O4 and [20]AneO4N4 ligands

results are in excellent agreement with those observed experimentally.

Ground-state multiplicities of the M^{2+} complexes and their relative stability

Ni^{2+} octahedral complexes are well-established high-spin complexes where the stability is highly dependent on the strength and symmetry of the ligand field [36]. It can be observed in Table 3 that the gap between singlet and triplet states of both complexes is higher for the complexation with oxygens than with nitrogen atoms, 31 and 23 kcal.mol^{-1}, respectively. Although the stronger ligand field induced by the nitrogen atoms reduces the energy difference between the low- and high-spin states, complexes where oxygen is the donor atom are still the most stable ones.

Table 2 Selected theoretical bond distances (Å) and bond angles (°) of complex **1a** for Ni^{2+} ion compared with the corresponding experimental (X-ray) values

	DFT/B3LYP	Experimental[a]	$\Delta_{DFT-exp}$[b]
N1-Ni	2.134	2.098	0.036
N2-Ni	2.127	2.111	0.016
Ni-O_{2W}	2.110	2.110	0.000
Ni-O_{1W}	2.100	2.120	−0.020
N1-Ni-N2	85.981	93.100	−7.119
N1-Ni- O_{2W}	88.191	89.720	−1.529
N2-Ni- O_{1W}	88.127	88.560	−0.433
O_{1W} -Ni- O_{2W}	179.996	179.960	0.036

[a] Ref. 10

[b] The difference between DFT and experimental results

Co^{2+} complexes represent a different situation and due to the d^7 electronic configuration and Janh-Teller distortion, degenerate electronic states are expected in the quartet multiplicity [37, 38]. In Co^{2+} **1a** complex, where nitrogen is the donor atom, quartet state is only 4.9 kcal.mol^{-1} more stable than the doublet one. A different aspect is seen for **1b** where quartet state is almost four times more stable than Co^{2+} **1a** conformation. In previous work, Aakesson *et al.* [37] observed that doublet-quartet gap is about 35 kcal.mol^{-1} for hexahydrated cobalt complexes.

Fe^{2+} is a more challenging case due to the fact that complexes can exist in quintet, triplet or singlet states. In Fe^{2+} **1b** complex, due to the oxygen atoms, the high-spin quintet state is considerably more stable than either the triplet or the singlet states. A different feature is seen for Fe^{2+} **1a** complexes where stability can be quintet > singlet > triplet state, although triplet−singlet gap is considerable small, almost 4 kcal.mol^{-1}. This value is also in good agreement with those observed by Guell *et al.* [39]. Guell *et al.* [39] showed that singlet−quintuplet gap for Fe^{2+} structures ranges from 7.9 to 21.7 kcal.mol^{-1}. Nevertheless, when the singlet state is the most stable one, the quintuplet−singlet gap is seen around 3.8−18.5 kcal.mol^{-1}.

It is important to mention here that the ligand field has a strong influence on the relative stability over the different electronic states. The weaker field promoted by the oxygen atoms is not enough to stabilize the lower multiplicity states in the case of Fe^{2+} complexes, therefore the singlet and the triplet states render much less stable structures than the quintet one. Based on these results, important aspects can be assigned on the first row M^{2+} cation complexes (Fe^{2+}, Co^{2+} and Ni^{2+}) since higher spin states are always more stable than those with lower multiplicity. In addition, the energy difference between several spin states is larger for **1a** complexes than **1b** structures. An explanation for this characteristic may be due to the stronger ligand field promoted by the nitrogen atoms which preferentially stabilizes the lower spin states.

For the second set of transition metals (Ru^{2+}, Rh^{2+} and Pd^{2+}), lower spin states are the most stable ones. The differences observed in the relative stability between the several electronic spin states on the first and second row complexes may be a consequence of two cooperating effects: (i) strong overlap between the large 4d orbitals and the ligand ones, and (ii) the decreasing pair energy due to the larger "volume" available for electrons in the 4d orbitals. Both effects may contribute to stabilize the low spin multiplicities [36]. In addition, the energy gap between **1a** and **1b** structures is larger than what is seen in the first row complexes. This gap, for the most stable states, ranges from 46 to 53 kcal.mol^{-1}, while in the first row structures these values decrease to 32−35 kcal.mol^{-1}.

Table 3 Absolute energies (a.u) and relative energies (kcal.mol^{-1}) for different multiplicities

M^{2+} cation	Multiplicity	Abs. energy (a.u.)	ΔE^a (kcal.mol^{-1})	Abs. energy (a.u.)	ΔE^a (kcal.mol^{-1})	Rel. energy^b (kcal.mol^{-1})
		1[a]		1b		1b – 1a
Fe^{2+}	Quintet	−1269.12043	0.00	−1269.10241	0.00	11.31
	Triplet	−1269.10812	9.99	−1269.06582	22.96	26.54
	Singlet	−1269.11386	6.38	−1269.05778	28.00	35.19
Co^{2+}	Quartet	−1290.76032	0.00	−1290.72953	0.00	19.32
	Doublet	−1290.75248	4.92	−1290.70062	18.15	32.54
Ni^{2+}	Triplet	−1314.98938	0.00	−1314.94938	0.00	25.10
	Singlet	−1314.95251	23.14	−1314.89998	31.00	32.96
Ru^{2+}	Quintet	−1239.46233	55.50	−1239.44882	13.53	8.48
	Triplet	−1239.50641	27.84	−1239.45335	10.69	33.30
	Singlet	−1239.55077	0.00	−1239.47038	0.00	50.44
Rh^{2+}	Quartet	−1255.09091	41.87	−1255.06258	13.10	17.78
	Doublet	−1255.15763	0.00	−1255.08346	0.00	46.54
Pd^{2+}	Triplet	−1272.33689	26.72	−1272.28612	5.82	31.86
	Singlet	−1272.37948	0.00	−1272.29538	0.00	52.77

[a] Calculated relative energies for the metals studied here, taking into account the most stable spin state as reference

[b] The relative energy difference between [20]AneN$_4$O$_4$ (**1a**) and [20]AneO$_4$N$_4$ (**1b**) complexes

Metal ion selectivity

la and **lb** complexation interaction energies are presented in Fig. 2. The **la** interaction energies are stronger than in the **lb** arrangements, as indicated in Table 3 by direct comparison of the energy differences among **la** and **lb** complexes. From Fig. 2 we can see that the interaction strength increases with the metal atomic number, i.e., Ni^{2+}>Co^{2+}>Fe^{2+} and Pd^{2+}> Rh^{2+}>Ru^{2+}, respectively to each row. Then, from Fig. 2 we can observe that the second row complexes bind always stronger than their corresponding first row metals. A similar behavior is also detected in **1b** complexes. An exception is seen for the Fe^{2+}/Ru^{2+} pair, where Fe^{2+} complex shows a binding energy 20 kcal.mol^{-1} higher than the Ru^{2+} ones. Considering the distances between metal ion and the water molecules it is possible to see that they are basically the same for all the compounds performed in this work. The higher discrepancy is seen in Pd^{2+} **1a** complex, which shows a bond length of 2.5 Å while the other second-row **1a** complexes present values ranging from 2.0 to 2.2 Å. Nevertheless, from Fig. 3 we can see that the average distance between metal ions and nitrogen and oxygen macrocyclic atoms gets shorter as the interaction between them becomes stronger; in other words, metal−ligand distances decrease as the atomic number increases in the periodic row. Also from

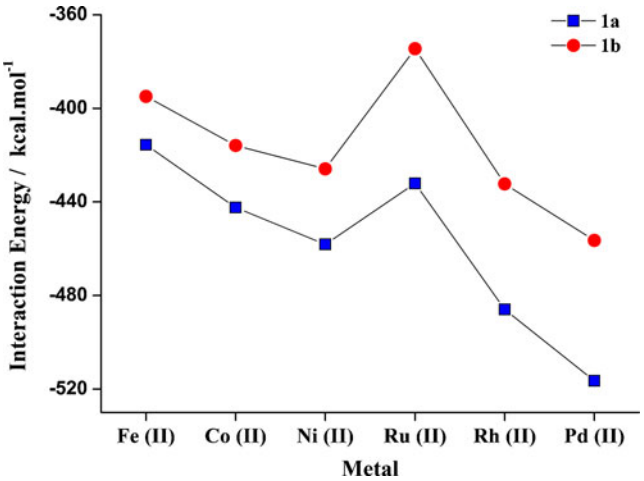

Fig. 2 Interaction energies as function of metal-ligand (ligand = nitrogen and oxygen) distances

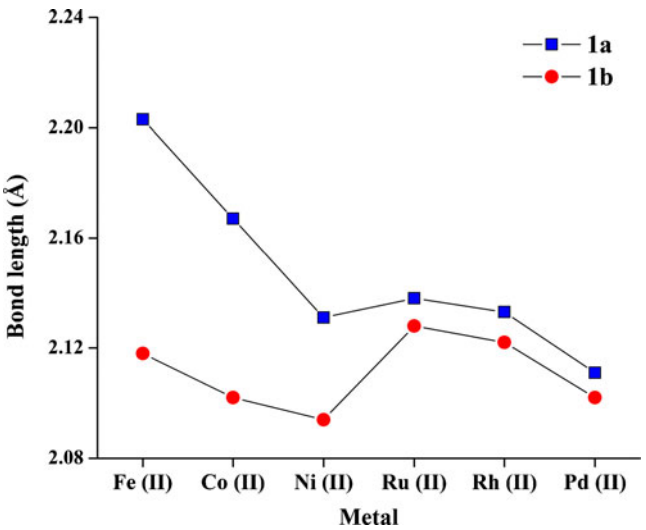

Fig. 3 Selected bond lengths between metal-nitrogen (**1a**) and metal-oxygen (**1b**)

Table 4 Charge decomposition analysis, difference in electronic polarization (PL) between metal and ligand fragments, charge transfer (CT) between fragments and net charge on metal and ligand for the closed shell macrocyclic complexes (all results in a.u)

Complex	Ru (1a)	Ru (1b)	Pd (1a)	Pd (1b)
Ligand-metal-donation	0.664	1.054	0.903	1.200
Metal-ligand back-donation	−0.020	−0.020	0.037	0.004
PL (metal) – PL (ligand)	78.7	68.9	51.3	38.0
CT (2→1) - CT (1→2)	1.284	1.392	1.513	1.567
Metal q_{NBO}	0.686	0.961	0.865	1.122
Atom donor q_{NBO}	−0.344	−0.477	−0.382	−0.477
O_{water} q_{NBO}	−0.929	−0.960	−0.998	−1.039

Fig. 3, we can see that [20]AneN_4O_4 macrocycle seems to be more rigid (with a less accessible conformation involved), which may lead to a lower level in the pre−organization. Therefore, with the metal complexation, an increase of the macrocycle field strength is expected, which increases the overlap metal−ligand bond (as will be discussed in the next section).

A molecular view of the chemical bond between metal ions and ligands

The **1a** and **1b** orbital contributions can be divided into three parts: (i) σ or π donation from the metal ligand fragment to the metal; (ii) π-back-donation from the metal to the ligand fragment, and (iii) electronic polarization of the metal and the ligand. The polarization of fragments is the effect of distortion of the electron distribution of one fragment by another one and includes the interactions between all permanent charges, charge multipoles and induced multipoles [37, 38]. Extended charge decomposition analysis (ECDA) method [38] was used to analyze charge transfer (CT) and polarization contributions individually. Donation, back-donation, charge transfer, polarization and NBO charges results on the metal and the ligand for **1a** and **1b** macrocyclic complexes of the closed and open-shell forms for the most stable multiplicity are given in Tables 4 and 5, respectively. In all cases the back-donation is very small, with contribution of only 0.01-0.04 (a.u) in both complexes, i. e., the back-donation is practically negligible, as could be expected for these typically σ-type ligands.

As it is well known, the chemical bond in transition metal complexes is usually described in terms of ionic and covalent interactions between the metal and the ligands, especially in first-row transition metals where ionic contribution is dominant [36]. As can be seen from Tables 4 and 5,

Table 5 Charge decomposition analysis, difference in electronic polarization (PL) between the metal and the ligand fragments, charge transfer between fragments and the net charge on the metal for the open-shell macrocyclic complexes in the most stable multiplicity state (all results in a.u.)

Complex	1a				1b			
	Fe	Co	Ni	Rh	Fe	Co	Ni	Rh
Ligand-metal donation$^{\alpha}$	0.602	0.650	0.663	0.244	0.628	0.684	0.710	0.568
Metal-ligand back-donation$^{\alpha}$	−0.044	−0.020	−0.017	0.011	−0.046	−0.028	−0.025	−0.016
Ligand-metal donation$^{\beta}$	0.793	0.792	0.804	0.617	0.800	0.812	0.801	0.696
Metal-ligand back-donation$^{\beta}$	0.004	0.011	0.011	0.022	0.007	0.005	0.005	0.000
$\Sigma^{\alpha+\beta}$ donation	1.395	1.442	1.467	0.963	1.428	1.496	1.511	1.264
$\Sigma^{\alpha+\beta}$ back-donation	−0.040	−0.009	−0.006	0.033	−0.039	−0.023	−0.020	−0.016
PL^{α} (metal) – PL (ligand)	−6.7	−6.9	−7.0	58.8	−6.8	−6.8	−6.9	27.7
PL^{β} (metal) – PL (ligand)	80.2	99.7	76.2	−0.1	80.1	121.1	108.6	29.9
$\Sigma^{\alpha+\beta}$ PL	73.5	92.8	69.2	58.7	83.3	114.3	101.7	57.6
CT^{α} (2→1) - CT (1→2)	1.007	1.043	1.065	1.247	0.987	1.046	1.009	1.316
CT^{β} (2→1) - CT (1→2)	1.446	1.598	1.793	1.469	1.402	1.514	1.656	1.533
$\Sigma^{\alpha+\beta}$ CT	2.453	2.641	2.858	2.716	2.387	2.560	2.665	2.849
Metal q_{NBO}	1.516	1.476	1.406	0.889	1.581	1.559	1.522	1.041
Atom donor q_{NBO}	−0.478	−0.475	−0.434	−0.374	−0.560	−0.563	−0.562	−0.501
O_{water} q_{NBO}	−1.035	−1.029	−1.026	−1.006	−1.071	−1.065	−1.055	−0.987

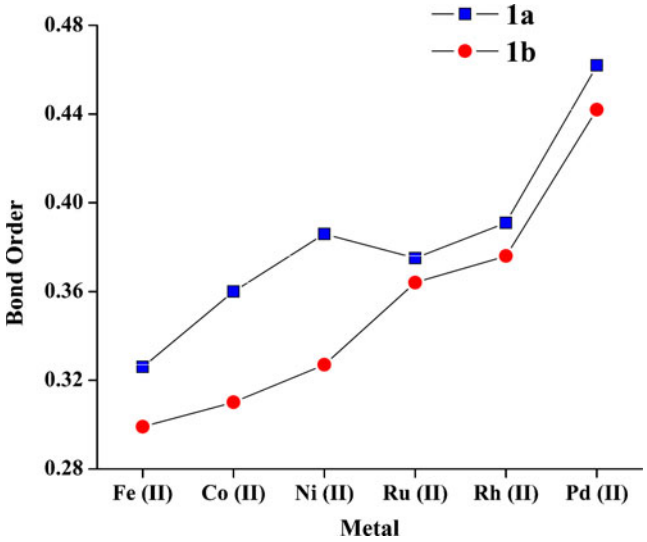

Fig. 4 The M-N and M-O bond order for **1a** and **1b** system, respectively

first−row transition metals complexes show significant covalent contribution. The intensity of the covalent interaction (charge donation) increases from Fe^{2+}<Co^{2+}<Ni^{2+}. This increase occurs simultaneously with the decreasing of the ionic contribution, as observed in Tables 4 and 5. The ionic contribution is related to the atomic charges of the metal and nitrogen (or oxygen) atoms from macrocycles. Also from Tables 4 and 5, we can see that the absolute values of the metal and ligand charges are higher in Fe^{2+} complexes, while they are lower in the Ni^{2+} ones. Therefore, the ionic interaction increases from Ni^{2+}<Co^{2+}<Fe^{2+}. The atomic charge in water molecule ligands was not taking into account, basically because it was almost constant for all complexes performed in this work.

Second-row transition metal complex analyses from NBO charges show that covalent contribution becomes stronger as compared to its corresponding first row ones. For example, Pd^{2+} **1a** HOMO-LUMO gap is 3.50 eV, while Ru^{2+} is 4.10 eV. Therefore, the strong covalent interaction is seen for the Ru^{2+} **1a** complex while Pd^{2+} **1a** structure presents the weaker covalent interaction for the second row, i.e., the high effective nuclear metal atom charge reduces the metal-ligand covalent interactions. In the case of Rh^{2+} **1a** complex an intermediate value (3.76 eV) is observed. The first row complexes present higher values for the covalent interaction than those observed in the second-row ones. Fe^{2+}, Co^{2+} and Ni^{2+} **1a** HOMO-LUMO gaps are 5.58, 5.96 and 6.10 eV, respectively. In other

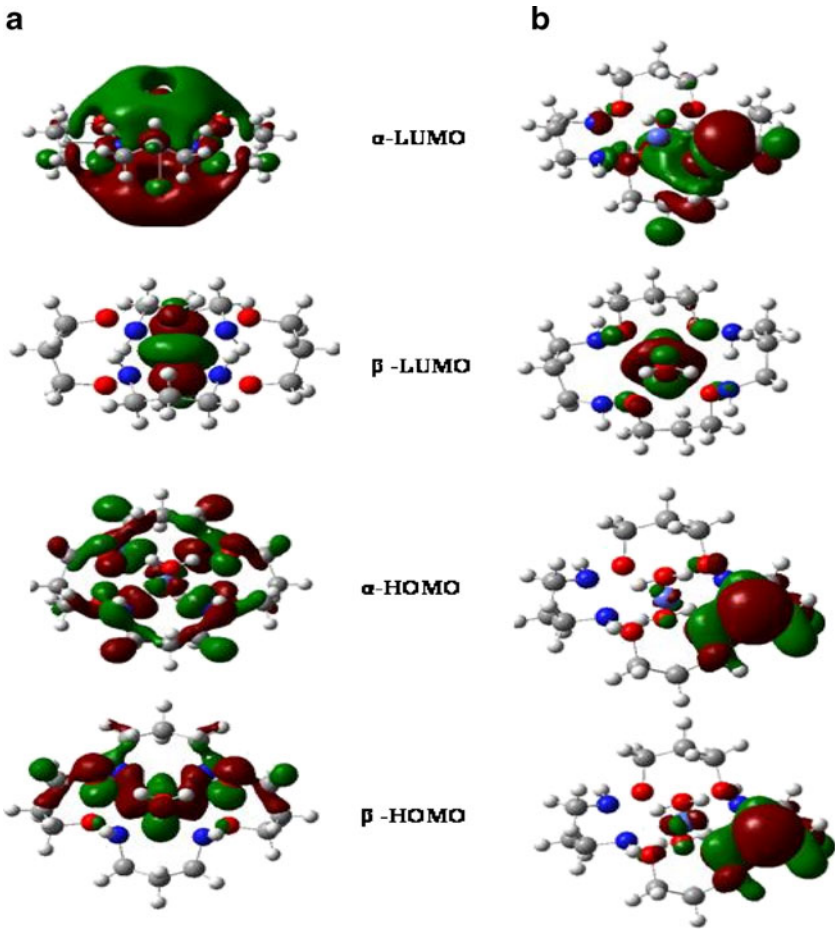

Fig. 5 Frontier α- and β-spin molecular orbitals for **1a** and **1b** complexes

words, the ionic contribution is predominant for first-row transition metals complexes, which is in good agreement with literature [40].

The high stability of **1a** complexes may also be correlated with the Mayer bond order. Figure 4 shows that the bond order increases as the atomic radii decrease. Therefore, there is a higher charge transfer (see Tables 4 and 5) between both fragments, which leads to stronger complexes. In all cases, the bond order is higher in **1a** complexes than in **1b** ones.

Molecular orbital (MO) representations are shown in Figs. 5 and 6. These MOs are relevant for chemical bonding and also to comprehend the high stability of complexes **1a** as compared to complexes **1b**. An important aspect is the similarity between first and second-row transition metals MO ordering. The **1a** α-HOMO is highly symmetrical; with an average of 30% 3d metal character while 70% is from macrocycle character. The α-LUMO orbitals are built up by a metal p_z and a macrocycle sp orbital, while the β−LUMO orbitals are dominated by the 3d metal orbital. In β MOs, the HOMO has the same character as that of the α-HOMO (although with lower symmetry). Otherwise, HOMO, HOMO-1 and HOMO-2 present a 3d metal character, while HOMO-3 shows the same character as that for α-HOMO. An analysis of **1b** frontier orbitals shows that α-HOMO, α-LUMO and β-HOMO orbitals are highly unsymmetrical. In fact, all **1b** orbitals are unsymmetrical and this influences the susceptibility of the metal ion orientations toward heteroatoms orbitals. In other words, the **1a** symmetric characteristics may reduce the energy cost for the macrocycle pre−organizations when the metal complexation occurs and, therefore, makes **1a** complexes more stable than the **1b** corresponding ones.

Vibrational frequency characterization

The assignments for the fundamental infrared bands of **1a** and **1b** complexes are demonstrated in Table 6 and 7, respectively. Vibrational frequency analyses were also performed and the **1a** and **1b** asymmetric (ν_{as}) and symmetric (ν_{sym}) stretching water features were assigned in the 3616−3700 cm^{-1} region. Making a comparison between both arrangements is possible to see that **1b** ν_{sym} and ν_{as} water stretching shows a downshift of 16−61 cm^{-1}, while the higher downshift was observed to Ru^{2+} **1a** complex. It is important to mention that these values are higher than those determined experimentally, which range

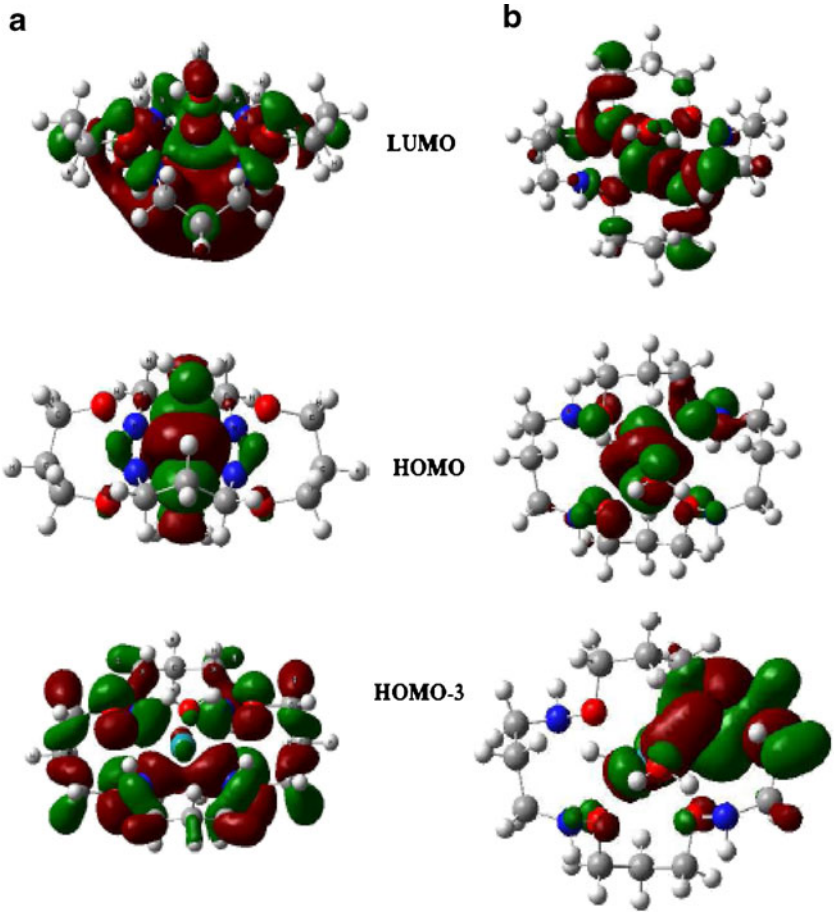

Fig. 6 Frontier molecular orbitals for the closed-shell **1a** and **1b** complexes

Table 6 The assignments for the fundamental infrared bands of **1a** complexes

[20]aneN4O4	Fe^{2+}	Co^{2+}	Ni^{2+}	Ru^{2+}	Rh^{2+}	Pd^{2+}	Assignments
–	3662	3675	3646	3667	3648	3699	$\nu_{as}(OH_2)$
–	3534	3514	3505	3537	3423	3547	$\nu_s(OH_2)$
3324	3293	3308	3297	3280	3269	3260	$\nu_s(NH)$
3021–2950	3043–2985	3045–2986	3047–2987	3044–2985	3048–2990	3055–2981	$\nu_{as}(CH_2)$
2942–2828	2970–2937	2973–2938	2975–2939	2972–2938	2976–2942	2978–2942	$\nu_s(CH_2)$
	1538	1534	1539	1538	1514	1550	$\sigma(OH_2)$
1488–1435	1476–1439	1476–1444	1477–1445	1473–1442	1471–1442	1473–1436	$\sigma(CH_2)$
1431–1325	1382–1306	1384–1327	1386–1327	1378–1326	1392–1325	1375–1323	$\delta_s(CH_2)$, $\delta_s(NH)$/
1243–1170	1272–1144	1275–1145	1278–1152	1284–1160	1284–1160	1278–1152	$\delta_d(CH_2)$
1130–975	1104–986	1103–954	1104–955	1102–1020	1105–1028	1133–1038	δ_s(C–C), ν_s(C–C), ν_s(C–N), ν_s(C–O–N)
967–660	960–716	938–720	935–723	955–699	960–724	963–726	δ_d(C–C), ν_{as}(C–N), ν_{as}(C–O–N), $\delta_d(OH_2)$
–	546	573	591	618	663	–	$\delta_s(OH_2)$
556–200	539–200	548–200	563–200	568–200	577–200	572–200	$\delta_d(OH_2)$, δ_d(C–C–C), δ_d(C–C–N), δ_d(C–N–O)
–	435	441	450	548	551	562	ν_s(M–N)
–	338	339	353	404	–	–	$\nu_{as}(M–OH_2)$
–	272	276	290	367	–	–	$\nu_s(M–OH_2)$

in 3200–3450 cm^{-1} region [41, 42]. Besides, the differences between calculated and experimental values may be due to the absence of a scale factor.

The N–H ν_{sym} frequency is observed in 3324 and 3237 cm^{-1} for [20]AneN4O4 and [20]AneO4N4, respectively. The latter complex presents a value close to that detected experimentally by Billes and Varady [43] to protoporhyrin IX (3246 cm^{-1}). This result is also in good agreement with other studies [42, 44–46]. It is important to mention that while an upshift after the complexation of **1a** complexes is observed, a downshift is seen in **1b** ones. Nevertheless, when we considered the CH_2 ν_{as} and ν_{sym} modes a decrease is expected in the band area of these two modes after the complexation, this is seen for **1a** and **1b** complexes which are mainly due to the fact that this mode is sensitive to conformation changes [41–46].

The H_2O scissoring vibrational mode (σ) is observed in 1535–1568 cm^{-1} region. The values from CH_2 σ mode enlarges after the metal coordination, however this shift is higher when considered the **1b** conformations. Besides, while the CH_2 deformation in-plane mode (δ_s) is detected in 1400 cm^{-1}, the NH δ_s is seen in 1300 cm^{-1}. Both δ_s mode

Table 7 The assignments for the fundamental infrared bands of **1b** complexes

[20]aneO4N4	Fe^{2+}	Co^{2+}	Ni^{2+}	Ru^{2+}	Rh^{2+}	Pd^{2+}	Assignments
–	3624	3639	3630	3616	3627	3653	$\nu_{as}(OH_2)$
–	–	–	–	–	–	–	$\nu_s(OH_2)$
3237	3258	3257	3255	3252	3270	3266	$\nu_s(NH)$
3020–2950	3041–2889	3046–2989	3049–2988	3045–2988	3049–2997	3064–2996	$\nu_{as}(CH_2)$
2944–2858	2972–2920	2972–2911	2971–2928	2970–2927	2975–2936	2977–2934	$\nu_s(CH_2)$
	1535	1542	1541	1545	1568	1771–1524	$\sigma(OH_2)$
1476–1422	1474–1429	1475–1434	1476–1433	1476–1437	1469–1432	1468–1430	$\sigma(CH_2)$
1417–1318	1427–1383	1427–1331	1427–1330	1429–1331	1420–1326	1420–1320	$\delta_s(CH_2)$, $\delta_s(NH)$/
1309–1160	1285–1171	1281–1179	1283–1179	1284–1181	1280–1173	1276–1170	$\delta_d(CH_2)$
1116–980	1118–1013	1120–975	1125–971	1126–971	1126–969	1123–961	δ_s(C–C), ν_s(C–C), ν_s(C–N), ν_s(C–O–N)
955–668	1004–660	948–676	940–670	940–670	932–668	930–643	δ_d(C–C), ν_{as}(C–N), ν_{as}(C–O–N), $\delta_d(OH_2)$
–	–	–	–	–	–	–	$\delta_s(OH_2)$
561–200	540–100	549–100	559–100	552–100	536–100	529–100	$\delta_d(OH_2)$, δ_d(C–C–C), δ_d(C–C–N), δ_d(C–N–O)
–	306	412	427	428	436	–	ν_s(M–O)
–	260	385	340	410	408	499	$\nu_{as}(M–OH_2)$
–	156	312	324	372	370	447	$\nu_s(M–OH_2)$

values, from CH_2 and NH, are valid for the ligand as the complex structure indicating that this mode is not very affected by the metal coordination. The H_2O δ_s is seen in 660 and 540 cm^{-1}, nevertheless for the first-row complexes this vibrational mode increases from Fe^{2+} to Ni^{2+}. In the second-row complexes, the H_2O δ_s vibrational mode is detected only for Ru^{2+} and Rh^{2+}, while for Pd^{2+} structures the values are higher due to the fact that water molecules are not coordinated to Pd atom, as it was previous explained.

The CH_2 deformation out of plane (δ_d) range from 1140−1300 cm^{-1} for **1a** and **1b** complexes, while Campos-Vallette *et al.* [44] observed these values between 1260−1280 cm^{-1} for Ni^{2+}, Cu^{2+} and Zn^{2+} azabipiridyl macrocyclic complexes. Besides, the CH_2 deformation found here in the plane (δ_s) is assigned in values close to 1400 cm^{-1}. Nevertheless, the C−C, C−N and C−O−N δ_s modes are observed in 955−1130 cm^{-1} region, which have been shown to be lower than the value detected by Diaz *et al.* [45] (~1300 cm^{-1}).

Nakamoto [46] showed that metal-nitrogen stretching ($\nu_{metal\text{-}N}$) occurs with values lower than 500 cm^{-1} and present small intensities, which has also been confirmed by other studies [42, 44–48]. These aspects were also observed in our DFT results, which are in good agreement with experimental $\nu_{Ni\text{-}N}$ results [44]. In the case of $\nu_{metal\text{-}O}$ stretching mode the contribution of this mode to the decreasing of metal-oxygen length can be observed, even to the first- as the second-row complexes. Nevertheless, in Pd **1b** complex the $\nu_{metal\text{-}O}$ is not detected which also enhances the fact the there is no bond formation between Pd and water molecules.

Conclusions

In this work we have studied the coordination ability of the oxa-aza macrocycle 1,7,1 l,17-tetraoxa-2,6,12,16-tetraaza-cycloeicosane with the several transition metal ions. The different coordination ability between the M^{2+} cations to bind with oxa-aza macrocylic ligand is attributed to an increase in the covalent nature of the metal-ligand chemical bond. Observing the HOMO-LUMO gap it can be seen that the ionic interaction increases from $Ni^{2+}<Co^{2+}<Fe^{2+}$, which is in good agreement with the fact that the ionic contribution is dominant in first-row transition metals. Nevertheless, covalent ones follow the respective order: $Pd^{2+}<Rh^{2+}<Ru^{2+}$. Examining the orbital representation it can be seen that all **1b** orbitals are unsymmetrical and this influences the susceptibility over metal ions orientation toward heteroatoms orbitals. In other words, the **1a** symmetric characteristic will reduce the energy cost for macrocycles pre−organization when the metal complexation occurs and, therefore, makes **1a** more stable complexes than **1b** corresponding ones.

Acknowledgments The author would like to acknowledge the financial support from FAPERJ (Fundação de Amparo à Pesquisa do Rio de Janeiro), CAPES (Coordenação de Aperfeiçoamento de Pessoal de Nível Superior) and CNPq (Conselho Nacional de Desenvolvimento Científico e Tecnológico).

References

1. Kimura E (1992) Macrocyclic polyamines with intelligent functions. Tetrahedron 48:6175–6217
2. Baumann TF, Reynolds JG, Fox GA (1998) Polymer pendant crown thioethers:synthesis and Hg-II extraction studies of a novel thiacrown polymer. Chem Commun:1637–1638
3. Kruper WJ, Rudolf PR, Langhoff CA (1993) Unexpected selectivity in the alkylation of polyazamacrocycles. J Org Chem 58:3869–3876
4. Takenouchi K, Watanabe K, Kato Y, Koike T, Kimura E (1993) Novel bifunctional macrocyclic chelating-agents appended with a pendant-type carboxymethylamino ligand and nitrobenzyl group and stability of the y-88(III) complexes. J Org Chem 58:1955–1958
5. De Clercq E, Yamamoto N, Pauwels R et al. (1992) Potent and selective-inhibition of human-immunodeficiency-virus (HIV)-1 and HIV-2 replication by a class of bicyclams interacting with a viral uncoating event. Proc Natl Acad Sci USA 89:5286–5290
6. Bridger GJ, Skerlj RT, Padmanabhan S, Thornton DA (1996) Versatile intermediate for the preparation of c-functionalized azamacrocycles and application to the synthesis of the potent Anti-HIV agent (+/−)JM2936. J Org Chem 61:1519–1522
7. Bridger GJ, Skerlj RT, Padmanabhan S et al. (1999) Synthesis and structure-activity relationships of phenylenebis(methylene)-linked bis-azamacrocycles that inhibit HIV-1 and HIV-8 replication by antagonism of the chemokine receptor CXCR4. J Med Chem 42:3971–398
8. Lin PKT, Araujo AN, Montenegro MCBSM, Perez-Olmos R (2005) New PVC nitrate-selective electrode:Application to vegetables and mineral waters. J Agric Food Chem 53:211–215
9. Hannongbua SV, Rod BM (1985) Quantum-chemical investigations on the interaction of alkaline-earth-metal ions with macrocyclic-compounds. Inorg Chem 24:2577–2580
10. Hancock RD (1990) Molecular mechanics calculations and metal-ion recognition. Acc Chem Res 23:253–257
11. Soto-Castro D, Guadarrama P (2004) Macrocyclic vs. dendrimeric effect. A DFT study. J Comput Chem 25:1215–1226
12. Freiria A, Bastida R, Valencia L, Macias A, Lodeiro C, Adams H (2006) Metal complexes with two tri-aza, tri-oxa pendant-armed macrocyclic ligands:Synthesis, characterization, crystal structures and fluorescence studies. Inorg Chim Acta 359:2383–2394
13. Inglez SD, Lima FCA, Silva ABF et al. (2007) Photoinduced electron-transfer processes based on novel Bipyridine-Ru(II) complex:Properties of cis-[Ru(2,2′-bipyridine)(2)(5,6-bis(3-amidopyridine)-7-oxanorbornene)](PF6)(2) and cis-[Ru(2,2′-bipyridine)(2)(3-aminopyridine)(2)](PF6)(2) complexes. Inorg Chem 46:5744–5753
14. Delgado R, Felix V, Lima LMP, Price DW (2007) Metal complexes of cyclen and cyclam derivatives useful for medical applications:a discussion based on thermodynamic stability constants and structural data. Dalton Trans 26:2734–2745
15. Inglez SD, Lima FCA, Camilo MR et al. (2010) Tuning of Photochemical and Photophysical Properties of [Ru-II(2,2′-bipyridine)(2)L-x] Complexes using Nonchromophoric Ligand Variations. J Braz Chem Soc 21:157–168
16. Kuksa V, Marshall C, Wardell S, Lin PKT (1999) The synthesis of novel oxa-azamacrocycles. Synthesis:1034–1038

17. Kuksa V, Marshall C, Wardell S, Lin PKT (2000) Synthesis and X-ray structures of Ni and Zn complexes of a novel oxa-azamacrocyclic system. Inorg Chem Commun 3:267–270
18. Hubin TJ (2003) Synthesis and coordination chemistry of topologically constrained azamacrocycles. Coord Chem Rev 241:27–46
19. Frisch MJ, Trucks GW, Schlegel HB et al. (2004) Gaussian 03, Revision C.02. Gaussian Inc, Wallingford, CT
20. Becke AD (1993) Density-functional thermochemistry.III. The role of exact exchange. J Chem Phys 98:5648–5652
21. Stephens PJ, Devlin FJ, Chabalowski CF, Frisch MJ (1994) Ab-initio calculation of vibrational absorption and circular-dichroism spectra using density-functional force-fields. J Phys Chem 98:11623–11627
22. Becke AD (1993) A new mixing of hartree-fock and local density-functional theories. J Chem Phys 98:1372–1377
23. Lee CT, Yang WT, Parr RG (1988) Development of the Colle-Salvetti correlation-energy formula into a functional of the electron-density. Phys Rev B 37:785–789
24. Vosko SH, Wilk L, Nusair M (1980) Accurate spin-dependent electron liquid correlation energies for local spin-density calculations - a critical analysis. Can J Phys 58:1200–1211
25. Farkas O, Schlegel HB (1998) Methods for geometry optimization of large molecules. I. An O(N-2) algorithm for solving systems of linear equations for the transformation of coordinates and forces. J Chem Phys 109:7100–7104
26. Farkas O, Schlegel HB (1999) Methods for optimizing large molecules. II. Quadratic search. J Chem Phys 111:10806–10814
27. Gorelsky SI, Lever ABP (2001) Electronic structure and spectral, of ruthenium diimine complexes by density functional theory and INDO/S. Comparison of the two methods. J Organ Chem 635:187–196
28. Gorelsky SI (1997) AOMix: Program for Molecular Orbital Analysis. York University: Toronto. Canada. http://www.sg-chem.net
29. Glendening ED, Bademhoop JK, Reed AE, Carpenter JE, Bohmann JA, Moraes CM, Weinhold F (1998) NBO 3.0. Theoretical Chem Institute, Madison, WI
30. Gorelsky SI, Ghosh S, Solomon EI (2006) Mechanism of N_2O reduction by the mu(4)-S tetranuclear Cu-z cluster of nitrous oxide reductase. J Am Chem Soc 128:278–290
31. Dapprich S, Frenking G (1995) Investigation of donor-acceptor interactions - a charge decomposition analysis using fragment molecular-orbitals. J Phys Chem 99:9352–9362
32. Mayer I (1983) Charge, bond order and valence in the *ab initio* SCF theory. Chem Phys Lett 97:270–274
33. Mayer I (1985) Bond orders and valences in the SCF theory - a comment. Theor Chim Acta 67:315–322
34. Mayer I (1986) On bond orders and valences in the *ab initio* quantum chemical theory. Int J Quantum Chem 29:73–84
35. Mayer I (1986) Bond orders and valences from *ab initio* wave-functions. Int J Quantum Chem 29:477–483
36. Miessler GL, Tarr DA (2003) In: Inorganic Chemistry.International, P H, Ed London, p 285
37. Akesson R, Pettersson LGM, Sandstroem M, Siegbahn PEM, Wahlgren U (1992) Theoretical *ab initio* SCF study of binding-energies and ligand-field effects for the hexahydrated divalent ions of the 1st-row transition-metals. J Phys Chem 96:10773–10779
38. Pierloot K, Delabie A, Ribbing C, Verberckmoes A, Schoonheydt RA (1998) Theoretical study of the structure and spectroscopic properties of cobalt(II) coordinated to six-rings in zeolites. J Phys Chem B 102:10789–10798
39. Guell M, Sola M, Swart M (2010) Spin-state splittings of iron(II) complexes with trispyrazolyl ligands. Polyhedron 29:84–93
40. Hubin TJ (2003) Synthesis and coordination chemistry of topologically constrained azamacrocycles. Coordin Chem Rev 241:27–46
41. Miller FA, Mayo DW, Hannah RW (2003) Course notes on the interpretation of infrared and Raman spectra. Wiley, New York 2003:297–355
42. Diaz G, Clavijo RE, Campos-Vallette MM, Saavedra M, Diez S, Munoz R (1997) Specular reflectance infrared spectra of the macrocycles cyclam and cyclamdione and their Cu(II) complexes deposited onto a smooth copper surface. Vibrat Spect 15:201–209
43. Billies F, Varady B (2008) A DFT study on the vibrational spectroscopy of protoporphyrin IX. Spectroc Acta A 70:729–734
44. Campos-Vallette M, Saavedra MS, Diaz GF, Clavijo RE, Martinez Y, Mendizabal F, Costamagna J, Canales JC, Garcia-Ramos JV, Sanchez-Cortes S (2001) Surface-enhanced vibrational study of azabipiridyl and its Co(II), Ni(II) and Cu(II) complexes. Vibrat Spect 27:15–27
45. Diaz GF, Campos-Vallette M, Saavedra MS, Clavijo RE, Canales JC, Costamagna J, Vargas J (2002) Surface vibrational study of macrocycle complexes:Co(II), Ni(II), Cu(II) and Zn(II) bis(phenylhydrazine)-1,10-phenanthroline. Vibrat Spect 28:223–234
46. Nakamoto K (1970) Infrared and Raman spectra of inorganic and coordination compounds, 2nd edn. Wiley, New York, pp 191–220
47. Chandra S, Pudir M (2007) Spectral studies of cobalt(II) complexes of 12-membered macrocyclic ligands having thiosemicarbazone moieties. Spectroc Acta A 68:883–890
48. Chandra S, Pudir M (2008) Spectroscopic characterization of chromium(III), manganese(II) and nickel(II) complexes with a nitrogen donor tetradentate, 12-membered azamacrocyclic ligand. Spectroc Acta A 69:1–7